ATOMIC STRUCTURE OF TILT BOUNDARIES IN Mo BICRYSTALS

J.-M. Penisson

JOURNAL DE PHYSIQUE
Colloque C5, supplément au n°10, Tome 49, octobre 1988

ATOMIC STRUCTURE OF TILT BOUNDARIES IN Mo BICRYSTALS

J.-M. PENISSON

Département de Recherche Fondamentale/Service de Physique, Centre d'Etudes Nucléaires, 85X, F-38041 Grenoble Cedex, France

Résumé. Différents joints de flexion dans des bicristaux de molybdène ont été observés en microscopie à haute résolution. L'utilisation d'une tension plus élevée (400 Kv) permet une meilleure résolution. Dans ces conditions la structure atomique de ces joints peut être déterminée de façon très précise et comparée à des modèles théoriques. La structure du coeur des dislocations primaires d'un joint de faible angle est en accord avec un modèle de coeur vide. Un joint d'angle fort en position presque symétrique a une structure facettée dans laquelle des unités structurales sont présentes alors que le meme joint en position très assymétrique ne présente plus ces unités structurales.

Abstract. Several tilt boundaries in Mo bicrystals have been observed by high resolution electron microscopy. The use of higher accelerating voltage leads to an increase of the resolving power. In these conditions the atomic structure can be precisely determined and compared to theoretical models. In a low angle boundary the core structure is in agreement with an empty core model. In a high angle boundary the structure is facetted and some structural units can be identified if the boundary is not too far from the symmetric position. A completely asymmetric boundary does not exhibit these structural units.

1. INTRODUCTION

An exact knowledge of the atomic structure of grain boundaries (GBs) is necessary for the understanding of their physical properties. This knowledge can be obtained by means of high resolution electron microscopy (HREM). Pure tilt boundaries observed along their common cristallographical axis are well suited objects for this investigation because the major part of the atomic relaxations lie in the observation plane. Tilt boundaries have been studied in gold (1) (2) (3) and in molybdenum (4). In the later case the study was performed at 200 Kv and the results were only qualitative, in particular no information on the core structure of the dislocations was obtained. In other cases extensive computer processing of the images was necessary to extract structural information. These results were limited by the relatively poor resolving power of the microscopes. The new high resolution microscopes have very good optical characteristics and they generally use higher accelerating voltages. This leads to an increase of the resolving power which then enables a complete interpretation of the atomic structure of GBs in metallic specimens in which the atomic spacings are in the 2 Å range.

2. HIGH RESOLUTION IMAGING CONDITIONS

2.1 General imaging conditions

A high resolution image contains information about the atomic positions in the specimen, but the relation between image and atomic structure is not always straightforward because the electronic wave function leaving the specimen is modified by the action of the microscope. Experimental images have to be compared to simulated ones in which the set of experimental parameters, namely : specimen thickness, defocus, spherical and chromatic aberrations, beam divergence, crystal orientation are taken into account. All these parameters have to be measured or at least estimated for each microscope (5).

There are two steps in image simulation :
The first one is the calculation of the interaction between the specimen and the incident electron beam. This is done using the well known multislice method (6). Amplitudes and phases at the exit surface are calculated with respect to specimen thickness. In general a perfect crystal is used for this calculation so that general conditions for HR observation can be readily determined. Calculations have been performed on [001] bcc Mo at 200, 400 and 800 Kv. The results show that the amplitude of 110 diffracted beams increases with accelerating voltage while the phase becomes more stable.

The second step is the calculation of the image itself which includes the practical conditions in which the picture has been taken. The ability of the microscope to give structure information is represented by the transfer function. For a crystalline specimen it has to take into account the dynamical phase shift between diffracted and non diffracted beams. It can be written in the simple case of 5 beams interference as (7) :

$$T = \cos(\chi_g - \chi_o - \frac{2\pi}{\lambda}(C_s\frac{\theta^4}{4} + \Delta z\frac{\theta^2}{2}))$$

where $\chi_g - \chi_o$ is the dynamical phase shift between the non diffracted beam and the g-diffracted beam.
C_s is the spherical aberration coefficient
Δz is the defocus.

A convenient way to describe the transfer function is to draw plots of T=+1 (white atomic positions) and T=-1 (black atomic positions) in a defocus-thickness diagram (Fig. 1).

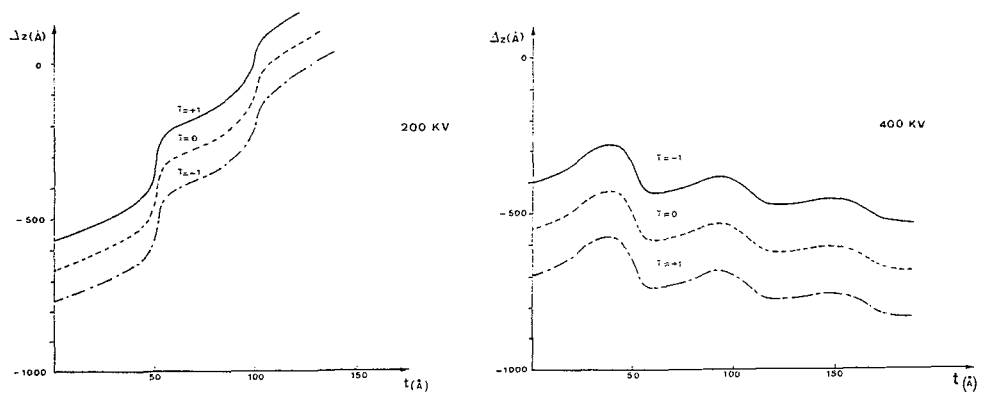

Fig. 1 :

From these plots it can be seen that a thickness variation of the specimen causes a rapidly oscillating contrast at 200 Kv while at 400 and 800 Kv the contrast is not affected in a large range of thicknesses. The transfer function is periodic with respect to defocus, the period being :
$2d^2/\lambda$ where d is the spacing of the imaged atomic planes and λ the electron wavelength.

The numerical values of this period for $d_{110}=2.2$ Å in Mo are listed below for each accelerating voltage

V(kV)	λ(Å)	$2d^2/\lambda$(Å)
200	.025	394
400	.016	616
800	.010	985

When the accelerating voltage is increased, the image periodicity is also increased so that the accuracy of focus setting and its measurement is less stringent. All the pictures have been taken at Scherzer defocus (defocus is measured on optical diffractograms). Specimen thickness is estimated to be in the 50 to 150 Å range. In these conditions the atomic positions are black.

The increase in resolving power has been experimentally checked on Mo single crystals. At 200 Kv only [001] and [111] projections of the structure can be imaged and defocus is much greater than Scherzer defocus so that the interpretation is delicate. At 400 Kv [001] and [111] projections of the bcc structure, respectively composed by two perpendicular and three 60° {110} atomic planes, are imaged at Scherzer defocus (-400 to -500 Å). [011] and [012] have also been imaged using larger defoci. In the later case two sets of {211} planes with d=1.28 Å are visible (Fig. 2).

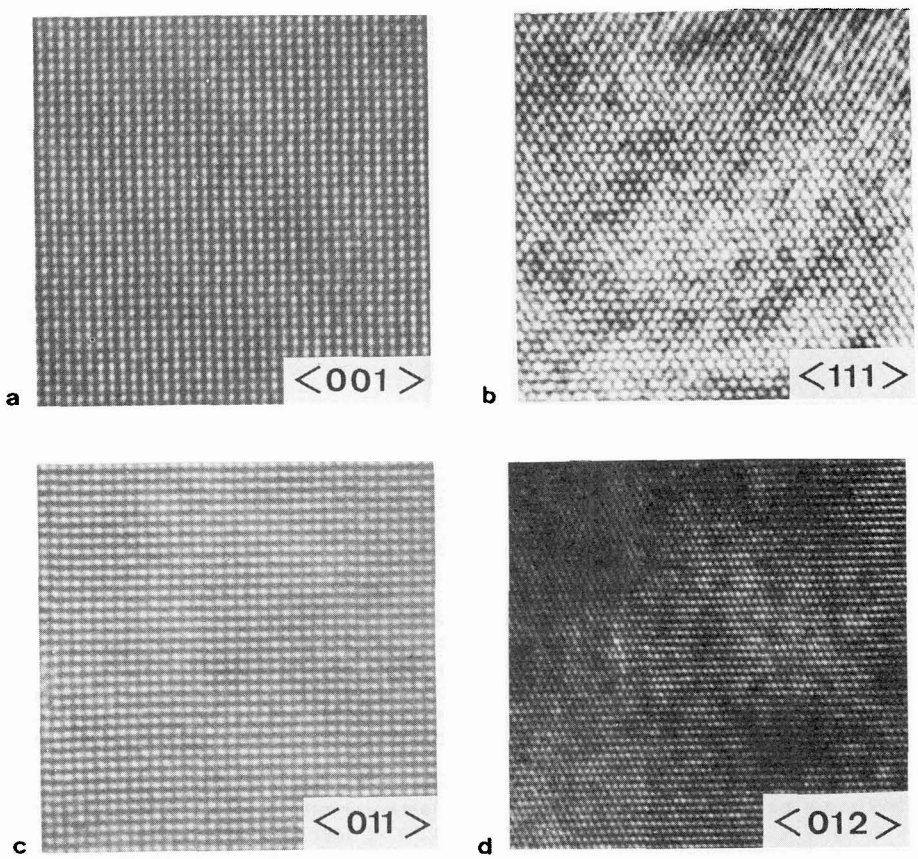

a b c d

Fig. 2 : Four different crystallographic projections of the bcc molybdenum structure (a=3.14 Å); JEOL 4000EX : 400Kv
a <001> projection showing two perpendicular sets of {110} planes (2.2 Å)
b <111> projection showing 3 sets of 60° planes
c <011> projection showing one set of {110} and one set of {200} (1.57 Å)
d <012> projection showing one set of {200} and two sets of {121} planes (d=1.28 Å)

2.2 Particular imaging conditions on GB

As high resolution images are related to the projection of the structure, the best specimens are those in which the atomic arrangement along the direction of projection is constant. This is why pure tilt boundaries are chosen for this work. A perfect specimen would then be a pure tilt boundary in which the grain boundary plane (GBP) is perfectly parallel to the incident beam. In fact, in the real specimens, there is always an additional misorientation angle which can be a small tilt or twist component. This extra angle can be observed and measured on an electron diffraction pattern in which the first Laue zone is visible (Fig. 3).

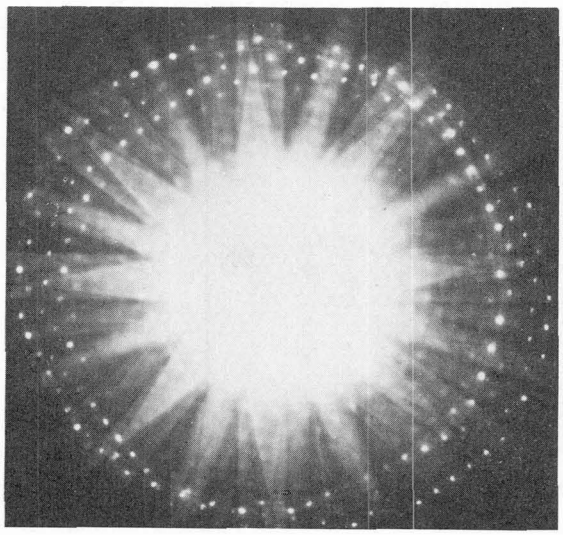

Fig. 3. Electron diffraction pattern taken on the GB : the first Laue circle is displaced because the $[001]_1$ and $[001]_2$ are not parallel.

The presence of this extra misorientation has two consequences :
i) The structure of the GB is more complicated : several sets of secondary dislocations may be necessary to accommodate the misorientation. Bollmann's theory of grain boundaries (8) allows to the determination of Burgers vectors, dislocation line and spacing of the secondary dislocations.
ii) The imaging conditions are more restricted. If one crystal is set at the exact Laue symmetrical position, the second will be tilted away from this position and the contrast changes or even disappears if the deviation angle is too large. Image simulation of a tilted crystal has shown that up to 4 mrad the tilt angle does not introduce a too large contrast change if the specimen is thin enough. In fact, the same contrast can be obtained if defocus is slightly changed. This means that a mean defocus value can in general be found for which contrast is the same on both crystals but this defocus is unique so that a through focus series is not possible.

If the GBP is not parallel to the incident beam, the two crystals overlap ; this effect leads to moire fringes : the atomic structure of the core is lost but information on the rigid translation can be extracted at least in the case of a twist boundary in which the GBP is perpendicular to the incident beam (9).

2.3 Image processing

At Scherzer defocus, atomic positions are black but intuitively the eye associates them with the white spots in the image. In order to improve the "readability" of the images, the range of intensity can be changed using computer processing so that the atomic positions appear as isolated black spots. At 400 kV constrast is very high and due to the brightness of LaB6 filament , noise is very low so that computer contrast enhancement is not in general necessary. In some cases, Fourier annular filtering can be used to eliminate some low spatial frequencies.

3. RESULTS FOR MOLYBDENUM TILT BICRYSTALS

Different types of tilt bicrystals have been elaborated and observed. The results reported here concern a low (14 degree) and a high angle (32 degree) tilt boundary around the common [001] direction.

3.1 Low angle boundary

The misorientation angle has been measured on HR images, electron diffraction and optical diffractogramms. Its value (14±1) degree is just between two major coincidences : Σ=25, 16.26° and Σ=41, 12.68°.

Geometrical description : Fig. 4 shows a general view of the boundary which appears relatively straight and is composed of discrete dislocations whose Burgers vectors are determined by means of Burgers circuits drawn around them. Two different types are present :

i) b=[100] dislocations. They are the most numerous ; they exhibit an extra half plane in each crystal and they are pure edge dislocations.
ii) b=1/2[111]. They are matrix dislocations in the bcc structure ; they have a mixed character. They are found from time to time in the boundary and are always associated with a step. Their screw component which cannot be determined from the pictures is responsible for the twist component of the misorientation angle.

The GB is straight and symmetric. Isolated dislocations are clearly visible. Careful inspection of the pictures shows that b=[100] dislocations are not equally spaced along the boundary. In order to measure their spacings, atomic positions are manually plotted from the black spots on transparent sheets. The dislocation cores appear as a capped triangular prism (10). They are separated from each other by a variable number of units of nearly perfect crystal. The comparison between the plots and calculated models shows that these different spacings represent the structural units describing the neighbouring coincidence GBs : Σ=25 and Σ=41 which correspond respectively to a dislocation core plus two or three square units. It should be noted that these two different structural units are mixed in a non periodic manner. Besides these simple structural units can find intermediate spacings with a non integer number of square units : 1.5, 2.5 or 3.5. In this case there is an atomic step in the boundary (fig. 5) and an associated secondary dislocation. The Burgers vector of the secondary dislocation and the step height are determined using a procedure given by King and Smith (11). The Burgers vector is b=a/41 [540] which is a base vector of the DSC lattice defined by Bollmann. It is a pure edge Burgers vector but it is not perpendicular to the GBP so that it introduces a step. It should be remarked that the Burgers vector of the secondary dislocation has been determined with respect to the Σ=41 coincidence as reference. The same determination can also been performed with the Σ=25 reference.

Comparison between experimental and simulated images : Σ=25 and Σ=41 coincidence boundaries have been modelised using a static method and an empirical interatomic potential (12). In these relaxation models, the dislocation core appears as a capped triangular prism but the prism can be either empty of filled with a molybdenum extra atom or with a foreign atom such as oxygen (13). For the filled core the energy of the boundary is higher than in the case of the empty core, but this eventuality has to be considered. Similar multiple structures have been found in copper (14) and in iron (15). The possibility of distinguishing between the two structures have been checked using computer simulation (16). The same kind of simulations in Mo bicrystals clearly showed that, at Scherzer defocus, the image of the empty core exhibits a typical feature : a white triangular spot which comes from the presence of a rather large tunnel in the structure . Some small differences in the atomic core atomic structure can appear for the different coincidence boundaries or models using different interatomic potentials but these differences do not affect the image. The exact intensity distribution varies with thickness and defocus but the general aspect remains unchanged. This feature can be observed in experimental images. From this convergence it can be concluded that the dislocation core is empty(Fig. 6).

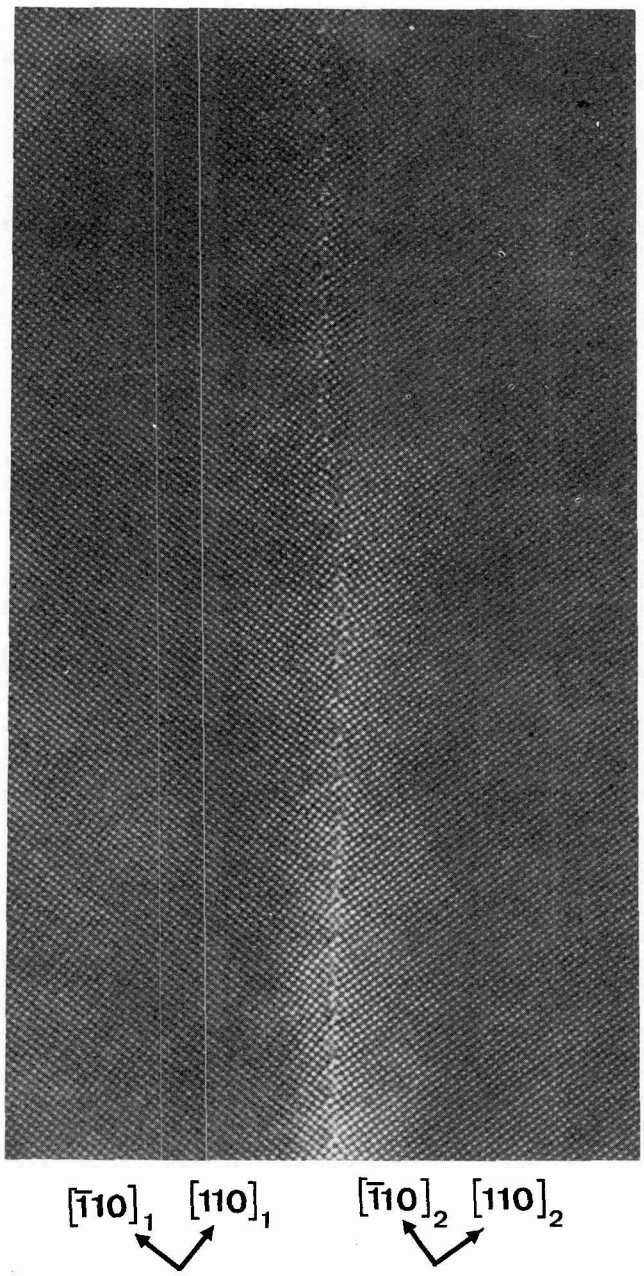

Fig. 4 : General HR image of a 14° grain boundary in Mo (JEOL 4000EX-400 Kv)

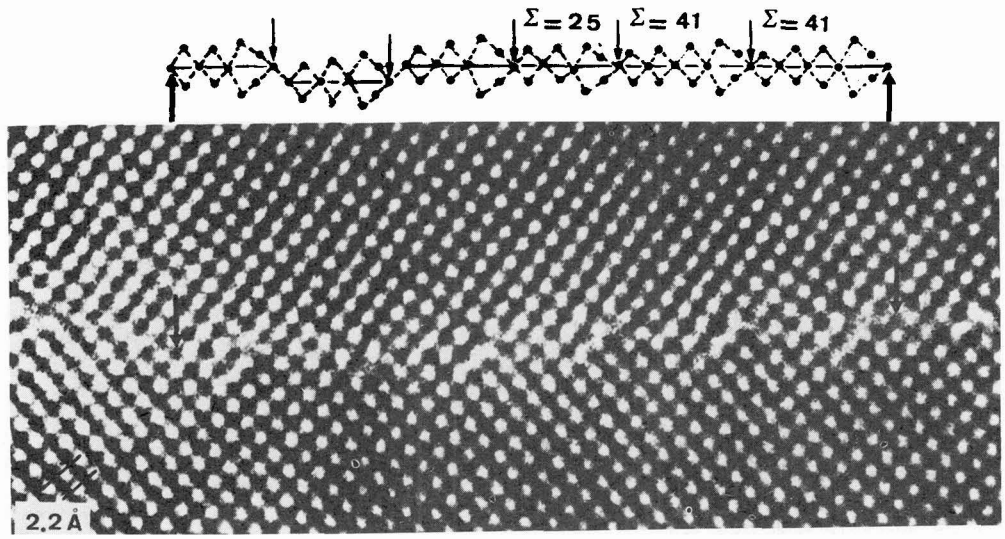

Fig. 5. Enlargement of fig. 4. The plot of atomic positions reveals the presence of Σ=25 and Σ=41 structural units together with atomic steps. Note that the arrangement is not periodic.

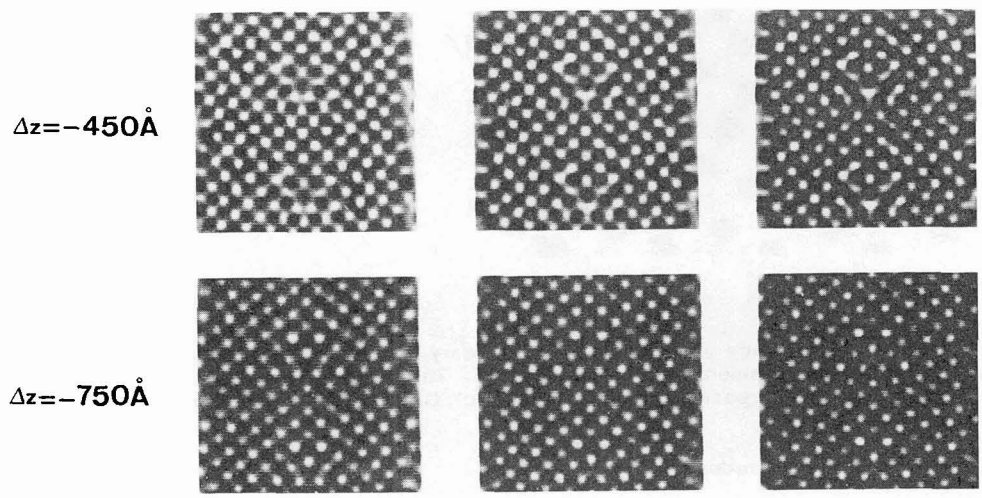

Fig. 6 : Σ=41 simulated images. The conditions are : C_s=1.05mm, beam divergence 0.7mrd, chromatic spread 70Å. These images correspond to a model in which the core is empty. A white triangular spot is present only at Scherzer defocus. This feature is present on experimental images.

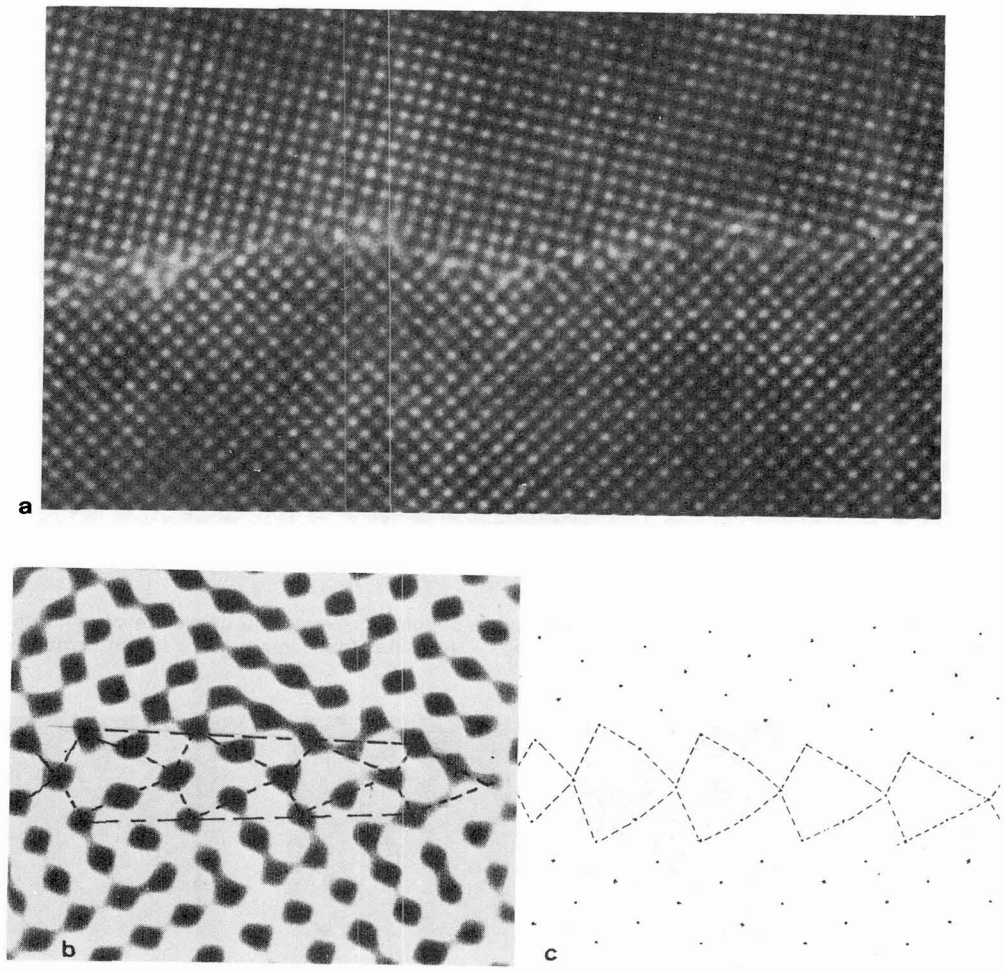

Fig. 7 (a) General image of a facetted 32° boundary. (b) Processed image of a symmetrical facet. The atomic positions are on black spots. The width of the structural units (capped triangular prisms) increases along the facet. (c) Geometrical model. (no atomic relaxation is present)

3.2 High angle boundaries

The observed boundary has a tilt angle e=32 degree around the common [001] axis. There also exists an additional 2 degree angle coming from the fact that the [001] axis of both crystals are not parallel. Due to the presence in the bicrystal of an array of subgrain boundaries, the GBP as well as the tilt angle changes. Some portions are in a nearly symmetric position while others are completely asymmetric.

The nearly symmetric boundary : it appears to be facetted. Small facets in symmetric position are connected to each other by portions of the boundary where the structure is not well defined. In the symmetric facets up to 4 capped triangular prisms can be aligned along a (720) plane : they are adjacent to each other and they are empty although some images

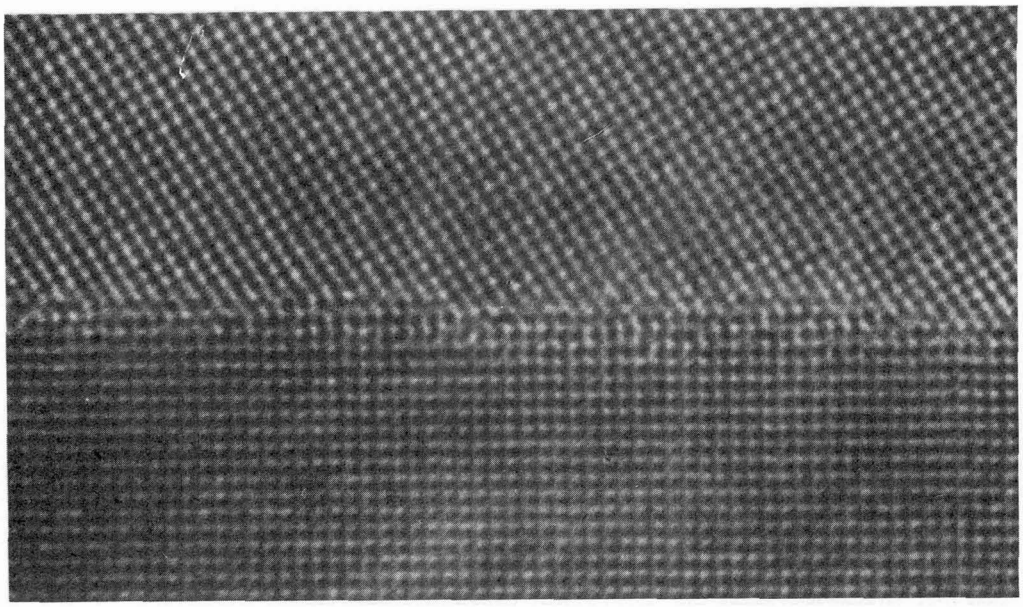

Fig. 8 : 32° asymmetric boundary

reveal an extra atom position in their center. A careful inspection of these structural units reveals that they are not strictly identical : their width measured in a direction perpendicular to the boundary is not constant ; it increases regularly along the facet (fig. 7). The tilt angle is 4 degree less than the Σ=5 coincidence so that the symmetric facets can be interpreted as portions of a nearly Σ=5 (310) boundary. In the exact coincidence boundary the 310 atomic planes are parallel in both crystal. Bishop and Chalmers (17) showed in a geometrical model that in a near Σ=5 boundary these planes are no longer parallel and the structural units are distorted. 310 atomic planes have been drawn in both crystals, their angle is about 4° which corresponds to the deviation angle with respect to the exact Σ=5 coincidence. In fact the tilt angle corresponds to the Σ=53, 31.9° coincidence. A simple geometrical model of the boundary shows exactly the same variation of the width of the structural units and simulated images from this model are very similar to the experimental ones.
The symmetric facets are separated from each other by asymmetric portions of various lengths. The boundary plane generally follows a low index plane of one of the two crystals and no structural units can be identified. The twist component of the misorientation is concentrated in these asymmetric facets.

Asymmetric boundary : the GBP is nearly parallel to 110 plane of one crystal (Fig. 8). Some atomic steps are present. No real periodicity can be found and only good fit areas are present in which atomic planes are continuous accross the GBP. No structural units can be found and up to now no model of such a boundary has been calculated. The observed boundary exhibits some similarity with the one observed in NiO by Merkle and Smith (18).

4. CONCLUSION

High resolution electron microscopy has now a resolving power consistent with the observation and the interpretation of tilt boundaries in metals and alloys in which the atomic spacings lie in the 2 Å range. Two types of information can be extracted from high resolution images :

Geometrical features such as Burgers vectors, spacing of the dislocations, presence of steps ; this type information does not require the exact location of the atomic positions in the GB and can be interpreted by means of geometrical theories such as that developped by

Bollmann. Low angle tilt boundaries around a common [001] axis are found to be composed of a non periodic mixing of structural units belonging to the neighbouring coincidences. This enlightens the problem of the choice for a reference in the description of a GB. In fact this choice is not unique. The observed high angle boundaries are facetted if the GBP is not too far from the symmetric position. Symmetric facets are separated from each other by non symmetric portions where the secondary dislocation needed to accomodate the deviation angle are located. If the GB is far from the symmetric position, the boundary plane is parallel to a low index plane of one of the two crystals. This is an indication that the surface energy plays an important role.

Structural information : The exact atomic positions are necessary for comparison with calculated models. When this comparison is made, the specimen quality plays a major role. In particular the misorientation has to be perfectly controlled which is not usually the case. Until recently it has only been possible to measure and to take into account the deviation angle from an exact coincidence . In fact pure tilt boundaries deviating from the exact coincidence contain more information than the exact ones because of the presence secondary dislocations, atomic steps and facetted structure. The GBP has to be exactly parallel to the incident beam. This point has to be carefully checked before the correct interpretation can be obtained. In particular dislocation rotations under the influence of the surfaces and mutual interactions between dislocations can introduce artefacts leading to an incorrect interpretation : some images previously attributed to a dissociation into partial dislocation are in fact inclined dislocations(19).
In low angle boundaries, comparison between experimental and simulated images shows that the dislocation core is empty which corresponds to a lower energy of the boundary. In high angle boundaries structural units are present in symmetric facets and their width increases along the facet. In asymmetric boundaries the results are not clear and a theoretical model is needed.

REFERENCES

1) F. COSANDEY, C.L. BAUER, Phil. Mag. **44**(1981)391
2) H. ICHINOSE, Y. ISHIDA Journal de Physique (1985)C4-39
3) W. KRAKOW, J.T. WETZEL, D.A. SMITH, Phil. Mag. **A53**(1986) 739
4) J.M. PENISSON, R. GRONSKY, J.B. BROSSE, Scripta Met. **16**(1982) 1239
5) A. BOURRET, J.M. PENISSON, JEOL News, 1987
6) J.M. COWLEY, Diffraction Physics, North Holland 1975
7) J. DESSEAUX, A. RENAULT, A. BOURRET, Phil. Mag. **35**(1977) 357
8) W. BOLLMANN Crystal Defects and Crystalline Interfaces Springer Verlag 1970
9) W. MADER, GF. NECKER, S.E. BABCOCK, R.W. BALLUFFI, Scripta Met, **21**(1987) 555
10) V. VITEK, D.A. SMITH, R.C. POND, Phil. Mag. **41**(1980) 649
11) A.H. KING, D.A. SMITH, Acta Cryst. **A36**(1980) 335
12) G. HASSON, Y. BOOS, I. HERBEUVAL, M. BISCONDI, C. GOUX, Surface Science **31**(1972) 115
13) T.N. NOWICKI, J.M. PENISSON, M. BISCONDI, this conference
14) V. VITEK, Y. MINONISHI, G.J. WANG, Journal de Phys. **46**(1985)C4-171
15) Y. MINONISHI, V. VITEK, S. MORZUMI, GB Structure and related phenomena Minakami, p. 245, 1986
16) W. WUNDERLICH, M. RUHLE 11thInt. Cong. on Electron Microsc. Kyoto vol. 2, 1335, 1986
17) G.H. BISHOP, B. CHALMERS, Phil. Mag. **29**(1971) 515
18) K.L. MERKLE, D.J. SMITH, Ultramicroscopy **22**(1987) 57
19) J.M. PENISSON, A. BOURRET, Phil. Mag. **40**(1979) 811